https://doi.org/10.5194/egusphere-2023-1131
Preprint. Discussion started: 6 July 2023

Effects of Arctic sea-ice concentration on turbulent surface fluxes in four atmospheric reanalyses

Tereza Uhlíková[1], Timo Vihma[2], Alexey Yu Karpechko[2], and Petteri Uotila[1]

[1]Institute for Atmospheric and Earth System Research, Faculty of Science, University of Helsinki, 00014, Helsinki, Finland
[2]Finnish Meteorological Institute, Helsinki, Finland

Correspondence: Tereza Uhlíková (tereza.uhlikova@helsinki.fi)

Abstract. A prerequisite for understanding the local, regional, and hemispherical impacts of Arctic sea-ice decline on the atmosphere is to quantify the effects of sea-ice concentration (SIC) on the turbulent surface fluxes of sensible and latent heat in the Arctic. We analyse these effects utilising four global atmospheric reanalyses: ERA5, JRA-55, MERRA-2, and NCEP/CFSR (CFSR and CFSv2), and evaluate their uncertainties arising from inter-reanalysis differences in SIC and in the sensitivity of the turbulent surface fluxes to SIC. The magnitude of the differences in SIC is up to 0.15, but typically around 0.05 in most of the Arctic over all four seasons. Orthogonal-distance regression and ordinary-least-square regression analyses indicate that the greatest sensitivity of both the latent and the sensible heat flux to SIC occurs in the cold season, November to April. For these months, the average sensitivity is 400 W m^{-2} for the latent heat flux and over 800 W m^{-2} for the sensible heat flux per unit of SIC (change of SIC from 0 to 1), with the differences between reanalyses as large as 300 W m^{-2} for the latent heat flux and 600 W m^{-2} for the sensible heat flux per unit of SIC. The sensitivity is highest for the NCEP/CFSR reanalysis. Comparing the periods 1980–2000 and 2001–2021, we find that the effect of SIC on turbulent surface fluxes has weakened, owing to the increasing surface temperature of sea ice and the sea-ice decline. The results also indicate signs of decadal-scale improvement in the mutual agreement between reanalyses. The effect of SIC on turbulent surface fluxes arises mostly via the effect of SIC on atmosphere-surface differences in temperature and specific humidity, whereas the effect of SIC on wind speed partly cancels out in the turbulent surface fluxes, as the wind speed increases the magnitude of both upward and downward fluxes.

1 Introduction

Interactive processes within the air-ice-ocean system play a key role in the rapid Arctic warming of the lower troposphere and sea-ice decline (Dai et al. (2002); Screen and Simmonds (2010); Serreze et al. (2009)). These processes are complex and challenging to represent in models, yet, to better understand the local, regional, and hemispherical impacts of Arctic sea-ice decline on the atmosphere, it is crucial to quantify the effects of sea-ice concentration (SIC) on turbulent surface fluxes in the Arctic.

The surface mass balance of sea ice (bare or snow-covered) is controlled by solar shortwave and thermal longwave radiative fluxes, turbulent surface fluxes of latent and sensible heat (LHF, SHF) as well as by conductive heat flux from the ocean through ice and snow. In winter, the cooling of the snow/ice surface due to negative net longwave radiation is balanced by downward

https://doi.org/10.5194/egusphere-2023-1131
Preprint. Discussion started: 6 July 2023

SHF from air to ice and upward conductive heat flux (Persson et al. (2002); Walden et al. (2017)). By warming the snow/ice surface, SHF reduces the temperature gradient through the ice and snow, and accordingly, reduces the basal ice growth (Lim et al., 2022). In spring, downward longwave radiation is usually the most important factor triggering the onset of snow melt on top of sea ice (Maksimovich and Vihma, 2012), whereas in summer, downward solar radiation is mostly responsible for the surface melt of snow and ice (Tsamados et al., 2015).

Sea ice affects the climate system by regulating the exchange of momentum, heat, moisture and other material fluxes between the atmosphere and the ocean, and having much higher albedo than the open sea. The difference in albedo between the sea ice and the ocean plays the most significant role during summer, when the sun is at its highest and the reduced albedo of the sea-ice-free water allows more absorption of the downward solar radiation that heats the ocean and, via the turbulent fluxes, the near-surface air (Perovich et al., 2007). The insulating effect of the sea ice is especially evident during winter and spring, when the ocean is considerably warmer than the atmosphere. The heat loss to the atmosphere then happens in leads, mostly governed by SHF, with smaller roles of LHF and net longwave radiation (Gultepe et al., 2003). The magnitude of upward LHF and SHF over these sea-ice openings is often ten to a hundred times larger than over the sea ice (Overland et al. (2000); Michaelis et al. (2021)); therefore, variations and climatological trends in SIC are critically important for the heat budget of the lower atmosphere and the upper ocean, and a key issue is to better understand and quantify the interactions of SIC and the surface turbulent fluxes.

From the point of view of modelling of the atmosphere, sea ice is a challenging surface type. SIC may change rapidly due to combined effects of dynamic and thermodynamic atmospheric and oceanic forcing (Aue et al., 2022). Due to these rapid changes and the challenges in sea-ice monitoring caused by the darkness during the polar night and prevailing cloud cover during summer, the information available on SIC is often inaccurate. Because of these optical challenges in the sea-ice monitoring, the information is mostly based on passive microwave remote sensing data from polar-orbiting satellites. However, as shown in Valkonen et al. (2008), the same passive microwave data processed using different algorithms may result in differences on the order of 20 %, which adds to the uncertainty in the representation of the arctic lower atmosphere in models.

Nevertheless, global atmospheric reanalyses provide the best available information in data-sparse regions such as the Arctic (Bosilovich et al. (2015); Gelaro et al. (2017); Kobayashi et al. (2015)), and are often relied upon in climate and climate-change research. These data sets aim to provide a physically consistent estimate of past states of the atmosphere with uniform spatial and temporal resolution around the globe, and they are generated by assimilating atmospheric and surface observations with short-term weather forecasts using modern weather-forecasting models. While the differences between reanalyses' variables of SIC, LHF, and SHF have been demonstrated via comparisons against observations (Bosilovich et al. (2015); Graham et al. (2019)) and inter-comparisons between reanalyses (Collow et al. (2020); Graham et al. (2019); Lindsay et al. (2014)), how much different reanalyses scatter in the relationships between SIC and surface turbulent fluxes is not known. To fill these knowledge gaps, we carry out an inter-comparison of four commonly-used major global atmospheric and coupled reanalyses: ERA5, JRA-55, MERRA-2, and NCEP/CFSR (coupled with the ocean), with a focus on their relationships between SIC, LHF, and SHF.

https://doi.org/10.5194/egusphere-2023-1131
Preprint. Discussion started: 6 July 2023

2 Material and Methods

The study region is the marine Arctic. We used data from the era of satellite measurements (1980–2021) as, compared to previous years, they provide more reliable and consistent information on the concentration of arctic sea ice, which in turn also allows for more precise estimation of turbulent surface fluxes in reanalyses. The past 42 years were divided into two study periods: 1980–2000 and 2001–2021. According to HadCRUT5 data (Morice et al., 2021), the Arctic has already been warming more than the world for most years since 1980, though, the Arctic amplification phenomenon strengthened considerably shortly after 2000. Hence, the division into two study periods allowed us to compare the period of the recent strong Arctic amplification of climate warming to the period directly preceding this phenomenon. Each year was divided into four three-month seasons with regard to the annual cycle of the Arctic sea ice: (1) November–December–January (NDJ), (2) February–March–April (FMA), (3) May–June–July (MJJ), (4) August–September–October (ASO). NDJ is represented by the months of high sea-ice extent, FMA by the months preceding and following the maximum sea-ice extent in March, MJJ by the months with low sea ice extent, and ASO by the months surrounding the month of minimum sea-ice extent in September.

We worked with data from four reanalyses: ERA5 (Hersbach et al., 2023), JRA-55 (JMA, 2013), MERRA-2 (GMAO (2015a); GMAO (2015b)), NCEP/CFSR (Saha et al. (2010), Saha et al. (2011)), all covering the selected period 1980–2021. Under the term 'NCEP/CFSR', we included data from NCEP Climate Forecast System Reanalysis (CFSR; covering the period 1980–2010) and NCEP Climate Forecast System Version 2 (CFSv2; covering the period 2011–2021). Because these two data sets come in different horizontal spatial resolutions (0.312°×0.313° resp. 0.204°×0.205°), we unified them for the whole data set 'NCEP/CFSR' to 0.4°×0.4° (∼45 km grid cell) using bilinear interpolation. Besides this adjustment, we worked with the original horizontal spatial resolution of the remaining reanalyses, which vary between ∼31 km to ∼55 km (ERA5, resp. JRA-55). The update cycle of reanalyses' forecasts (temporal resolution) ranges from 1 to 6 hours (ERA5 and MERRA-2, resp. NCEP/CFSR). In our study, we used daily means of the data as they provide sufficient representation of synoptic-scale atmospheric and sea-ice processes for our needs while significantly decreasing the size of the data set. For an overview of the basic characteristics of the reanalyses see Table 1.

From each reanalysis, we utilized the following variables: sea-ice concentration (SIC), surface latent heat flux (LHF), surface sensible heat flux (SHF), specific humidity in 2 m (Q_{2m}), temperature in 2 m (T_{2m}), temperature at the surface (T_s), U-component of wind (u), and V-component of wind (v), both in 10m. The signs of both turbulent heat fluxes were assigned with regard to the surface - positive LHF referring to condensation and deposition, negative to evaporation and sublimation; positive SHF referring to the downward flux, negative to the upward flux. Because Q_{2m} is not archived in ERA5 data sets, we followed Eqs. (7.4, 7.5) from ECMWF (2016) to calculate it using the dew-point temperature and surface pressure. Subsequently, we obtained the temperature difference between the surface and 2-m height (T_{diff}) by subtracting T_{2m} from T_s, and calculated the wind speed (WS_{10m}) using u and v. To obtain the difference in specific humidity between the surface and 2-m height (Q_{diff}), we first computed specific humidity at the surface (Q_s) according to Iribarne and Godson (1973) using T_s. For calculation of Q_{diff}, we then subtracted Q_{2m} from Q_s as in the case of T_{diff} calculation.

Using data from each reanalysis, we studied bilateral relationships between turbulent heat fluxes LHF or SHF and SIC,

https://doi.org/10.5194/egusphere-2023-1131
Preprint. Discussion started: 6 July 2023

Table 1. Basic characteristics of utilized global atmospheric and coupled reanalyses.

	ERA5	JRA-55	MERRA-2	NCEP/CFSR
Reference	Hersbach et al. (2020)	Kobayashi et al. (2015)	Gelaro et al. (2017)	Saha et al. (2010) Saha et al. (2014)
Forecast model	IFS CY41R2	JMA GSM	GEOS 5.12.4	GFS (Atmospheric model) MOM4 (Ocean model)
Data assimilation system	4DVar	4DVar	3DVar	3DVar (Coupled forecast system)
Horizontal resolution	0.25°×0.25° ∼31 km	0.561°×0.563° ∼55 km	0.5°×0.625° ∼50 km	CFSR: 0.312°×0.313° CFSv2: 0.204°×0.205° This study: 0.4°×0.4°; ∼45 km
Original temporal resolution	1 h	3 h	1 h	6 h

Table 2. Representation of the sea ice in reanalyses.

	ERA5	JRA-55	MERRA-2	NCEP/CFSR
Sea-ice concentration (SIC)	Fractional, external dataset[1]	Binary[2], external dataset[1]	Fractional, external dataset[1]	Fractional, modelled (coupled)
SST[3] for clearing the sea ice	3°C	None	None	2.15°C
Sea-ice thickness	1.5 m, fixed	2 m, fixed	N/A[4]	Modelled (coupled)
Snow on ice	None	None	None	Modelled (coupled)

[1] See text for details
[2] SIC > 0.55 = 1, SIC ≤ 0.55 = 0
[3] Sea-surface temperature
[4] 7-cm ice layer for computing a prognostic ice surface temperature, which is then relaxed towards 273.15 K as a representation of the upward oceanic heat flux.

and multilateral relationships between LHF (SHF), SIC, Q_{diff} (T_{diff}), and WS_{10m} – the three latter variables being selected based on the LHF and SHF bulk parameterisation. In reanalyses, the general bulk parameterisation of surface turbulent fluxes is grid-averaged, taking into account different surface types with different surface temperatures (Claussen (1991); Koster and Suarez (1992)). In our case, the different surfaces within a grid cell were the sea-ice and water, therefore the bulk formulae of grid-averaged LHF ($< E >$) and SHF ($< H >$) includes SIC as shown in (Vihma, 1995):

$$< E > = V\rho\, L_E[SIC(C_{E,ice}(q_{s,ice} - q_a)) + (1 - SIC)(C_{E,water}(q_{s,water} - q_a))] \quad (1)$$

https://doi.org/10.5194/egusphere-2023-1131
Preprint. Discussion started: 6 July 2023

$$< \mathrm{H} > = \mathrm{V}\rho\ \mathrm{c_p}[\mathrm{SIC}(\mathrm{C_{H,ice}}(\theta_{\mathrm{s,ice}} - \theta_{\mathrm{a}})) + (1 - \mathrm{SIC})(\mathrm{C_{H,water}}(\theta_{\mathrm{s,water}} - \theta_{\mathrm{a}}))] \quad (2)$$

where V stands for the wind speed at the lowest atmospheric level of the model applied in each reanalysis, ρ for the air density, L_E for the latent heat of sublimation, c_p for the specific heat of the air, and C_E, C_H for the turbulent exchange coefficients; (q_s - q_a) and ($\theta_{s,ice}$ - θ_a) are the differences in potential temperature and specific humidity between the surface and the lowest atmospheric level. In our study (specifically in Section 3.3), we apply true T_s and T_{2m} when studying their effect on SHF, because the adiabatic correction in a 2-m layer is negligible.

For the bilateral-relationship analysis, we utilised the orthogonal-distance regression (ODR; Boggs et al. (1988)). Because all variables in reanalyses include uncertainties, we theoretically considered the ordinary-least-square regression (OLSR), which assumes no errors in the independent variable, not optimal for this case. Additionally, we carried out tests on bilateral ODR and OLSR performance using data from several grid cells from each reanalysis and while we found nearly identical coefficients of determination (correlation coefficient squared, R^2) for both regression methods, importantly, the slopes of the regression lines varied considerably. This is attributable to the above-mentioned OLSR's assumption of no errors in the independent variable (x, in our case SIC) and therefore minimising the distance only for x data to the regression line, whereas ODR minimises the orthogonal distance between both x and y data (in our case y is LHF or SHF) and the regression line. For the case of multilateral regression analysis, however, we found nearly identical values for all slopes of the regression lines between LHF (SHF) and SIC, Q_{diff} (T_{diff}), and WS_{10m} for both ODR and OLSR. Values of R^2 for all and individual components of the multilateral regression were nearly identical using both ODR and OLSR as well. Based on these findings, we decided to use OLSR for the multilateral regression analysis, as it requires much fewer computing resources to perform. For both bilateral and multilateral regression analyses, we applied the linear regression model. While we were aware of some non-linearity in the SIC effect on Q_{2m} (T_{2m}) and LHF (SHF), we still evaluated it as the most applicable for our purposes.

The statistical-significance testing of the results (slopes for LHF, SHF and their explanatory variables) was performed using Student's t-test (95 % confidence interval) with adjusted degrees of freedom (DF_{adj}) according to Eq. (31) from Bretherton et al. (1999):

$$\mathrm{DF_{adj}} = \mathrm{T}\frac{1 - \mathrm{R_1 R_2}}{1 + \mathrm{R_1 R_2}} \quad (3)$$

where T stands for number of days in one sample (in our case days in seasons in the periods of 1980–2000 and 2001–2021) and R_1 respectively R_2 for correlation coefficient for lag 1 auto-correlation of turbulent heat flux (LHF or SHF and its explaining variable (SIC).

Each reanalysis typically uses not only its own (1) data-assimilation system, (2) forecast model (as seen in Table 1), and often (3) different parameterisation schemes for subgrid-scale variables (such as turbulent fluxes), but also more or less (4) different atmospheric and surface observations, and (5) different representations of the sea ice. In Table 2, we describe the representation of sea ice in selected reanalyses, which can have a considerable effect on the modelling of the lower troposphere. External datasets (unspecified in Table 2) used as sources for SIC in ERA5, JRA-55, and MERRA-2 are follows. ERA5

https://doi.org/10.5194/egusphere-2023-1131
Preprint. Discussion started: 6 July 2023

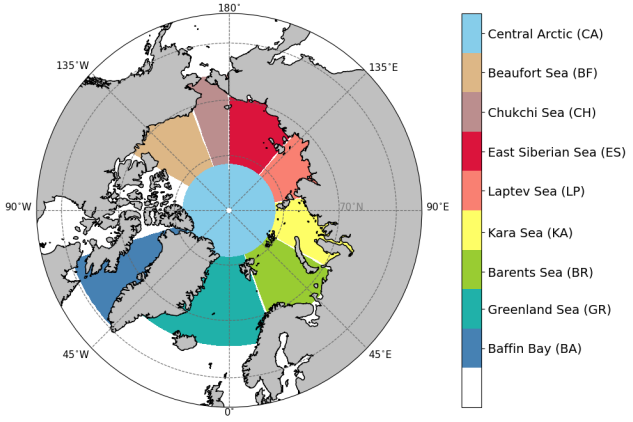

Figure 1. Arctic basins used for calculating daily field means of sea-ice concentration (SIC) and latent heat flux (LHF) in Tables 3, 4, S1, and Figures 2, 3, and S2.

uses data from OSI SAF (Ocean and Sea Ice Satellite Application Facility) by EUMETSAT (European Organisation for the Exploitation of Meteorological Satellites): version OSI SAF (409a) for January 1979 through August 2007, and OSI SAF oper for September 2007 onwards (Hersbach et al., 2020). In JRA-55, conditions for SIC are daily data from COBE-SST (Centen-
135 nial In Situ Observation-based Estimates of the Variability of Sea Surface Temperatures and Marine Meteorological Variables) (Kobayashi et al. (2015); (Matsumoto et al., 2006)). MERRA-2 uses monthly data from CMIP (Coupled Model Intercomparison Project) as in Taylor et al. (2000) prior to 1982, data from OISST (Optimum Interpolation Sea Surface Temperature) by NOAA (National Oceanic and Atmospheric Administration) for 1982 to March 2006, and data from OSTIA (Operational Sea Surface Temperature and Ice Analysis) by the Met Office from April 2006 onwards (Gelaro et al., 2017).

140 3 Results

3.1 Differences in sea-ice concentration and surface turbulent fluxes

To illustrate the climatology in and differences between the four selected reanalyses in sea-ice concentration (SIC), latent heat flux (LHF), and sensible heat flux (SHF), we calculated Mean Biases of daily field means (MBs) between ERA5 and other reanalyses (JRA-55, MERRA-2, NCEP/CFSR) in nine Arctic basins (Figure 1) in all seasons and the two study periods
145 (Figures 2, 3, and S2). We do not assume that ERA5 is the best reanalysis with respect to turbulent surface fluxes, but use MBs just for clarity of presenting comparisons. Mean values of ERA5 variables in these basins, seasons, and periods are shown in Tables 3, 4, and S1. For the calculations of both MBs and mean values, we used land-sea masks provided by each reanalysis and only considered grid cells completely covered by the sea.

The mean SIC in ERA5 ranged from 0.003 in Baffin Bay in ASO in 2001–2021 to 0.93 in the Central Arctic in FMA in
150 2001–2021. The value of mean SIC decreased in nearly all basins between the periods 1980–2000 and 2001–2021: by 1 to 48

https://doi.org/10.5194/egusphere-2023-1131
Preprint. Discussion started: 6 July 2023

Table 3. Mean sea-ice concentration in arctic basins as represented in ERA5 in 1980–2000 (I) and 2001–2021 (II).

Season	**NDJ**		**FMA**		**MJJ**		**ASO**	
Time period	I	II	I	II	I	II	I	II
Central Arctic	0.92	0.92	0.92	0.93	0.88	0.89	0.88	0.85
Beaufort Sea	0.60	0.60	0.61	0.61	0.53	0.51	0.50	0.37
Chukchi Sea	0.72	0.67	0.76	0.76	0.64	0.58	0.49	0.27
East Siberian Sea	0.74	0.73	0.75	0.74	0.66	0.62	0.57	0.32
Laptev Sea	0.35	0.35	0.36	0.35	0.30	0.26	0.23	0.13
Kara Sea	0.30	0.25	0.32	0.30	0.25	0.18	0.13	0.04
Barents Sea	0.23	0.12	0.31	0.21	0.18	0.09	0.05	0.02
Greenland Sea	0.13	0.10	0.15	0.12	0.10	0.08	0.07	0.05
Baffin Bay	0.19	0.15	0.25	0.23	0.14	0.11	0.01	0.00

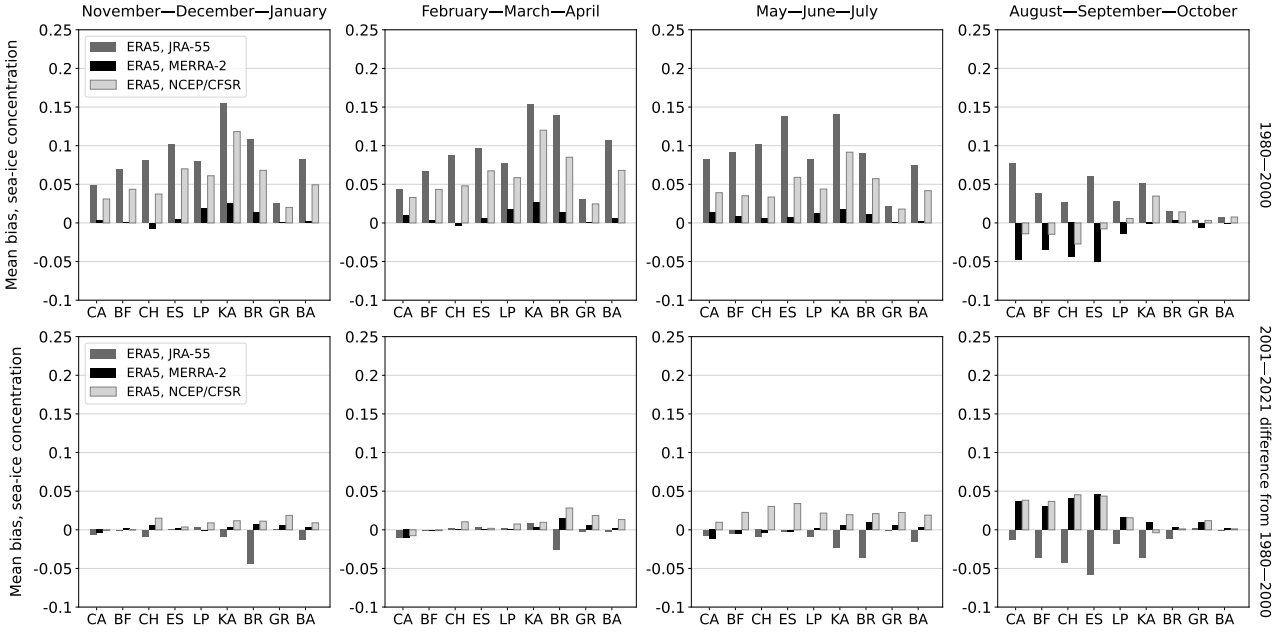

Figure 2. Mean biases of daily field means of sea-ice concentration between ERA5 and JRA-55 (grey), ERA5 and MERRA-2 (black), and ERA5 and NCEP/CFSR (light grey). Horizontal axis refers to arctic basins as seen in Figure 1. The first row shows data from period 1980–2000 and the second row the 2001–2021 difference from the earlier period. Only grid cells fully covered by the sea were considered in this analysis.

https://doi.org/10.5194/egusphere-2023-1131
Preprint. Discussion started: 6 July 2023

Table 4. Mean latent heat flux (W m^{-2}) in arctic basins as parameterised in ERA5 in 1980–2000 (I) and 2001–2021 (II).

Season	**NDJ**		**FMA**		**MJJ**		**ASO**	
Time period	I	II	I	II	I	II	I	II
Central Arctic	-3	-2	-3	-2	-11	-10	-5	-5
Beaufort Sea	-1	-2	-2	-2	-6	-6	-5	-6
Chukchi Sea	-5	-9	-2	-3	-7	-7	-11	-15
East Siberian Sea	-1	-2	-2	-2	-7	-7	-6	-8
Laptev Sea	-1	-1	-1	-1	-4	-3	-3	-5
Kara Sea	-2	-6	-1	-3	-3	-3	-5	-7
Barents Sea	-32	-37	-23	-30	-9	-10	-19	-20
Greenland Sea	-35	-36	-30	-32	-10	-12	-19	-20
Baffin Bay	-11	-14	-7	-9	-3	-3	-8	-9

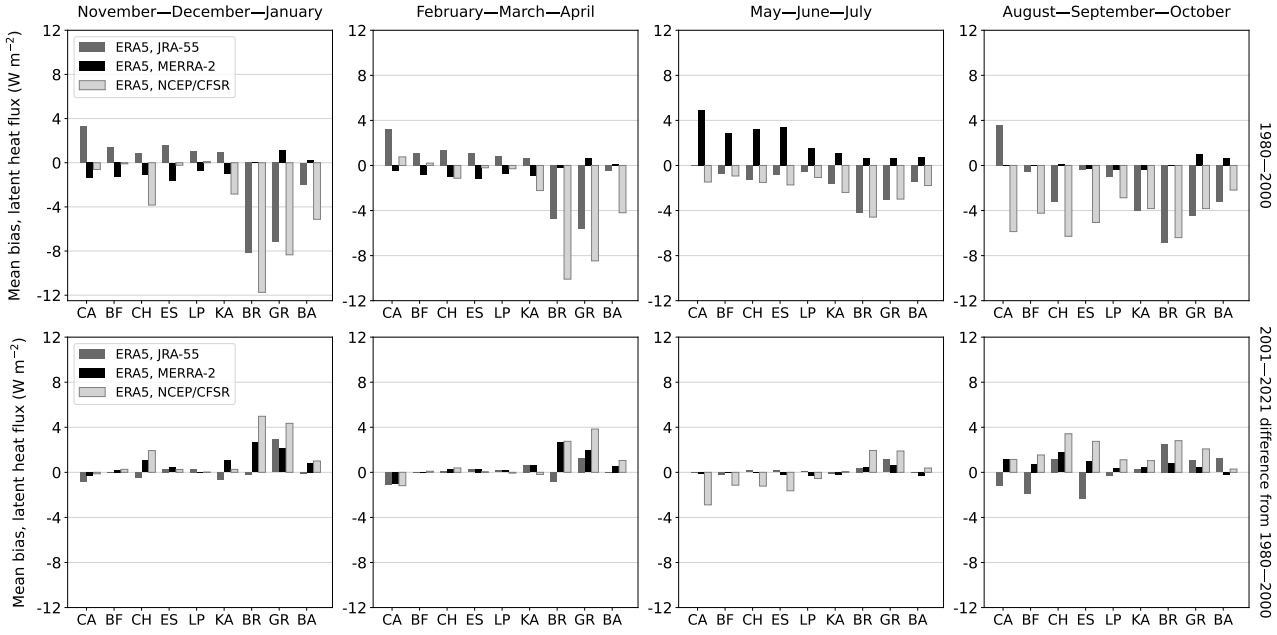

Figure 3. Mean biases of daily field means of latent heat flux between ERA5 and JRA-55 (grey), ERA5 and MERRA-2 (black), and ERA5 and NCEP/CFSR (light grey). Horizontal axis refers to arctic basins as seen in Figure 1. The first row shows data from period 1980–2000 and the second row the 2001–2021 difference from the earlier period. Only grid cells fully covered by the sea were considered in this analysis.

% in NDJ, 0.5 to 32 % in FMA, 5 to 51 % in MJJ, and 3 to 57 % in ASO. On the contrary, it increased or remained the same between the two study periods in the Central Arctic (in NDJ, FMA, and MJJ) and Beaufort Sea in NDJ and FMA, by up to

https://doi.org/10.5194/egusphere-2023-1131
Preprint. Discussion started: 6 July 2023

0.01.

The MBs of daily field means between ERA5 and other reanalyses (Figure 2) were in nearly all regions and seasons in 1980–2000 between -0.05 and 0.1, with almost all negative MBs in ASO, between ERA5 and MERRA-2, and ERA5 and NCEP/CFSR. For most of the data in 1980–2000, the differences between ERA5 and MERRA-2 were the lowest, almost exclusively within ± 0.03, and the differences between ERA5 and JRA-55 were the largest, up to 0.15 in the Kara Sea in NDJ and FMA. The large MBs between ERA5 and JRA-55 were expected given the binary representation of SIC in JRA-55 (assigning value 1 for over 0.55 of SIC in a grid cell, and 0 for equal or less than 0.55), as opposed to nearly all concentrations being considered in other reanalyses (ranging from 0 to 1 in MERRA-2 and from 0.15 to 1 in ERA5 and NCEP/CFSR). However, the MBs in SIC between ERA5 and NCEP/CFSR were also considerably high, rather closer to the differences between ERA5 and JRA-55 than those between ERA5 and MERRA-2. The magnitude of MBs between ERA5 and JRA-55, and ERA5 and MERRA-2 mostly decreased between the periods 1980–2000 and 2001–2021, whereas the differences in SIC between ERA5 and NCEP/CFSR systematically rose between these two periods in nearly all basins and seasons, closing the gap with JRA-55 MBs in the latter period, and even surpassing it in the Barents and Greenland Sea.

We found the mean LHF in ERA5 to be negative in all basins, seasons, and both periods (Table 4), with the smallest magnitude of the mean flux in the Laptev Sea (-0.8 W m^{-2}) in NDJ 1980–2000, and largest in the Barents Sea (-37 W m^{-2}) in NDJ 2001–2021. Corresponding to the changes in the mean SIC between the two study periods, in the cold seasons (NDJ, FMA), the mean negative LHF intensified in all the basins with decreased SIC and weakened in the Central Arctic. The mean negative LHF in MJJ weakened between the two study periods even in basins with smaller SIC – owing to warmer near-surface air temperatures in recent decades, allowing higher air specific humidity which reduces evaporation.

Values of MB in LHF between ERA5 and other reanalyses took place mostly between +5 and -10 W m^{-2} for the majority of basins and seasons (Figure 3). As in the case of SIC, the MBs between ERA5 and MERRA-2 were the lowest for most basins and seasons. The most noticeable results in the period 1980–2000 were large negative MBs during NDJ and FMA in the Barents and Greenland Seas between ERA5 and NCEP/CFSR, and ERA5 and JRA-55. These findings were not consistent with the theoretical expectations – positive MBs in SIC being followed by positive MBs in LHF (more sea ice resulting in less evaporation/sublimation than in ERA5). However, as we will show in the Section 3.2 (Figures 4 and S3), in NDJ and FMA, the correlations of SIC/LHF in NCEP/CFSR and JRA-55 are not of a different sign from ERA5 and do follow the theoretical expectations for this relationship. Because the sea ice covers only a small part of the Greenland and Barents Sea basins (even in NDJ and FMA) and we calculated the mean surface turbulent fluxes and MBs using the whole extent of each basin as shown in Figure 1, the larger negative LHF in NCEP/CFSR and JRA-55 (and to a lesser extent also in MERRA-2) compared to ERA5 are likely due to the differences in other factors affecting LHF (see Eq. (1)) in the ice-free areas of these basins.

The mean SHF in ERA5 ranged from +2 W m^{-2} in the Central Arctic in FMA 2001–2021 to -34.2 W m^{-2} in the Barents Sea in NDJ 1980–2000 (Table S1). The theoretical expectation for the cold seasons (NDJ, FMA) was, as in the SIC/LHF relationship, that the above-shown decline in SIC between the two study periods (Table 3) would result in stronger negative (upward) SHF from the (newly exposed) warmer ocean. This was the case in the majority of basins in these seasons, where the mean SHF was negative or zero in the first period and the SIC declined between the study periods. In ASO, we found mostly

https://doi.org/10.5194/egusphere-2023-1131
Preprint. Discussion started: 6 July 2023

stronger mean negative SHF in basins with previously negative mean SHF. As shown in Chung et al. (2021), the ocean in the Arctic begins to release absorbed summer heating from solar radiation in the autumn, when the air temperatures decrease. Because there has been considerably more summer heating of the ocean in the Arctic in recent decades due to the decline in SIC and surface albedo, we attribute the amplified negative SHF in this season in most basins to the above-described mechanism, which also works for LHF.

The MBs in SHF between ERA5 and other reanalyses (Figure S2) ranged approximately within ± 15 W m^{-2} for the majority of basins in NDJ and FMA, and ± 5 W m^{-2} in MJJ and ASO. MBs in MERRA-2 data in 1980–2000 were negative in nearly all seasons and basins, with largest magnitude in NDJ and FMA (up to -15 W m^{-2} in the Central Arctic in NDJ). JRA-55 and NCEP/CFSR showed mostly positive MBs in most basins and seasons (up to over +15 W m^{-2} in JRA-55 in Central Arctic), although, as in the case of LHF, the MBs in the Barents and Greenland Seas, and Baffin Bay were negative. The above-mentioned explanation of this seemingly non-physical relationship between positive MBs in SIC and negative MBs in the surface turbulent flux of latent heat applies in the case of SHF as well. Additionally, we show in Section 3.2 (Figures 6 and S6) that the SIC/SHF correlation is also of the same sign within all four reanalyses in our study. As to the MBs in SHF in 2001–2021 between ERA5 and JRA-55, MERRA-2, or NCEP/CFSR, their magnitudes decreased in nearly all basins and seasons, compared to 1980–2000.

3.2 Effect of sea-ice concentration on surface turbulent fluxes

To investigate the relationships between Arctic SIC and surface turbulent fluxes in reanalyses data, we first carried out bilateral orthogonal-distance-regression (ODR) analyses between SIC, LHF and SIC, SHF. For these analyses, we only included data (grid cells) with the mean of SIC > 0.5 in each period and season.

In Figure 4, we illustrate the change in LHF (W m^{-2}) per unit of SIC (slope of the regression line) in NDJ in the period 1980–2000 and the difference of 2001–2021 from 1980–2000. The relationship between SIC and LHF in the Arctic in these months showed solely positive correlation (shades of red in Figure 4: i–iv) meaning less sea ice – more evaporation/sublimation. This finding was consistent with the theoretical expectations: large amounts of moisture being released to the dry winter arctic air from the (relatively) warm ocean when it is exposed by the sea ice retreat. Although the direction of the relationship was the same in all four reanalyses, there were differences in its strength. While we found the slopes of regression lines between SIC and LHF to be around 200–300 W m^{-2} LHF per unit of SIC (change of SIC from 0 to 1) in ERA5, JRA-55 and MERRA-2, we observed values up to 600 W m^{-2} LHF per unit of SIC in NCEP/CFSR data, indicating much higher sensitivity of LHF to SIC in the marine Arctic in this reanalysis. The large dark grey areas in the JRA-55 results (Figure 4: ii and vi) indicate a failure of the linear bilateral ODR model, caused by the binary representation of SIC in this reanalysis. Because the SIC in these dark grey areas was never less than 0.55 during the 21-year periods, every grid cell was assigned a value of 1, making it impossible for the model to explain the variations in LHF by variations in SIC. In other reanalyses, the dark grey areas appear as well, analogically, due to very low SIC variability in some regions (we will address this matter further in detail later in this Section and in Figures 6 and 7).

A positive correlation between SIC and LHF could also be observed in FMA and ASO (shades of red in Figures S3 and

https://doi.org/10.5194/egusphere-2023-1131
Preprint. Discussion started: 6 July 2023

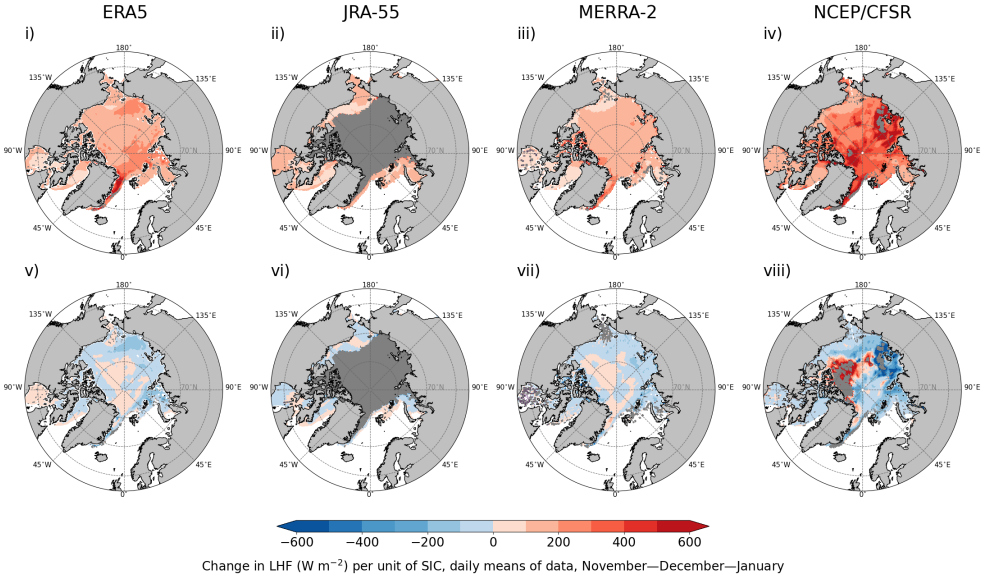

Figure 4. Change in latent heat flux (W m^{-2}) per unit of change in sea-ice concentration (slope of regression line) in four reanalyses (columns), marine Arctic, NDJ, based on the linear orthogonal-distance-regression (ODR) model. **i–iv** depict the period 1980–2000, **v–viii** show the 2001–2021 difference from 1980–2000. Dark grey indicates areas where the ODR model did not converge; in v–viii, dark grey shows these areas in 1980–2000 and/or 2001–2021. Only grid cells with a mean of SIC > 0.5 were considered, and only statistically significant results within 95 % confidence interval are shown.

S5: i–iv), with generally stronger relationship between the variables (about 300–600 W m^{-2} LHF per unit of SIC in ERA5 and NCEP/CFSR) than in NDJ. In MJJ, however, the relationship between SIC and LHF turned into a negative correlation in most areas, meaning less sea ice – less evaporation (shades of blue in Figure S4: i–iv). In this season, we found the strongest SIC/LHF relationship in the Central Arctic (north of 81.5 °N) for all reanalyses, ranging from around 300 W m^{-2} MERRA-2, to 400–600 W m^{-2} in ERA5 and NCEP/CFSR. The negative correlation between SIC and LHF in MJJ can be explained as follows. Based on various SIC thresholds, the reanalyses keep the sea-surface temperature relaxed to the approximate sea-water freezing point (-1.8 °C) throughout the year (e.g. in Ishii et al. (2005), Good et al. (2020)), often resulting in the open water being colder than melting snow/ice in summer with the surface temperature at 0 °C (Persson et al. (2002); Vihma et al. (2008); Walden et al. (2017)). Accordingly, the surface temperatures favor less evaporation over the open water than over melting sea ice.

The effect of SIC on LHF in all seasons (as parameterised in reanalyses) weakened between the two periods for most of the Arctic (shades of blue in Figures 4, S3, S5: v–viii; shades of red in Figure S4: v–viii). To interpret this change, we produced Figure 5, which shows that the surface temperature (T_s) has risen nearly everywhere in the marine Arctic between 1980–2021 (row x). The strongest surface warming in the Barents, Kara, Laptev, and Chukchi Seas can be attributed to the sea ice being to a large extent replaced by the warmer sea (see the areas of strongest sea-ice decline in row xi). The warming

https://doi.org/10.5194/egusphere-2023-1131
Preprint. Discussion started: 6 July 2023

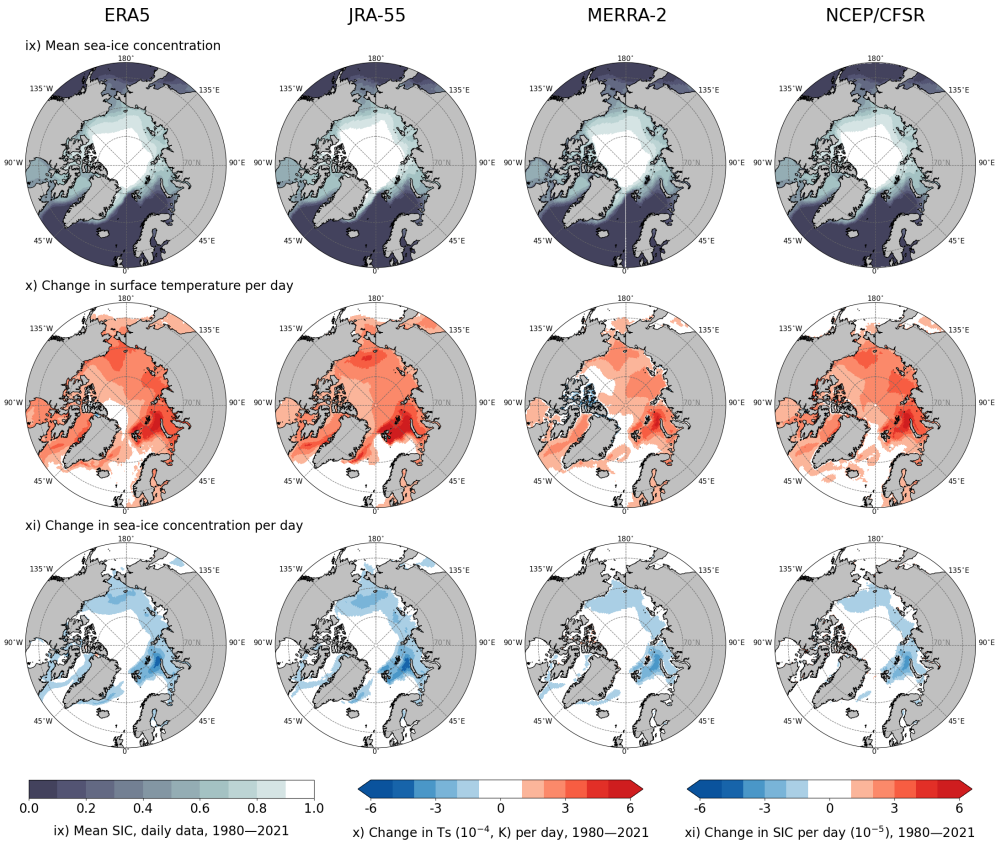

Figure 5. Mean sea-ice concentration (row **ix**), change of surface temperature per day (row **x**), and change in sea-ice concentration per day (row **xi**); 1980–2021, daily means of data in four reanalyses. Changes in variables per day are slopes of ordinary-least-square-regression line using time as an independent variable.

in other areas (including the Central Arctic, where the mean SIC in 1980–2021 was 0.9–1, see row ix) indicates warming of the sea-ice surface in past decades. Based on these findings, we present the following explanations on why the SIC/LHF relationship weakened between the two study periods: (1) For the leads opening in otherwise mostly compact sea ice: the surface temperature of the sea ice has increased while the underlying sea temperature remained the same (at the sea-water freezing temperature of approximately -1.8 °C), hence, the difference in the surface saturation specific humidities between the sea ice and open water decreased, directly contributing to a decreased sensitivity of LHF to SIC; (2) The sea ice has declined considerably or disappeared completely from some of the grid cells, therefore there is very small to no SIC effect on LHF in the latter study period. Mostly in the Central Arctic, however, we found large areas of increased SIC effect on LHF between 1980–2000 and 2001–2021 (shades of red in Figures 4, S3, S5: v–viii; shades of blue in Figure S4: v–viii, meaning a stronger relationship in 2001–2021). We interpret this change as a result of an increased variability of SIC in these areas in the latter

https://doi.org/10.5194/egusphere-2023-1131
Preprint. Discussion started: 6 July 2023

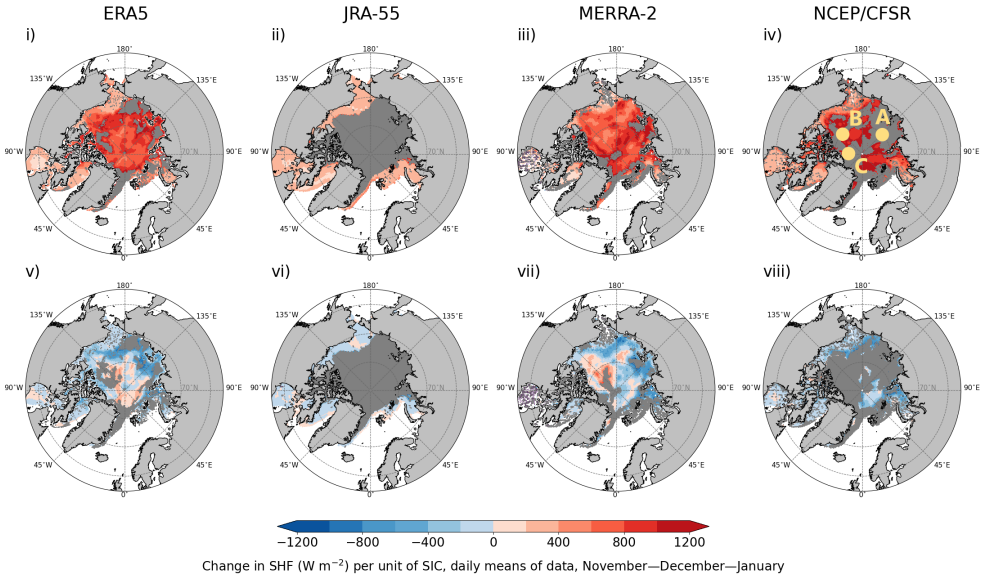

Figure 6. Change in sensible heat flux (W m^{-2}) per unit of change in sea-ice concentration (slope of regression line) as represented in four reanalyses (columns), marine Arctic, NDJ, based on the linear orthogonal-distance-regression (ODR) model. **i–iv** depict the period 1980–2000, **v–viii** show the 2001–2021 difference from 1980–2000. Dark grey indicates areas where the ODR model did not converge; in v–viii, dark grey shows these areas in 1980–2000 and/or 2001–2021. Points A, B, C from iv are further analysed in Figure 7. Only grid cells with a mean of SIC > 0.5 were considered, and only statistically significant results within 95 % confidence interval are shown.

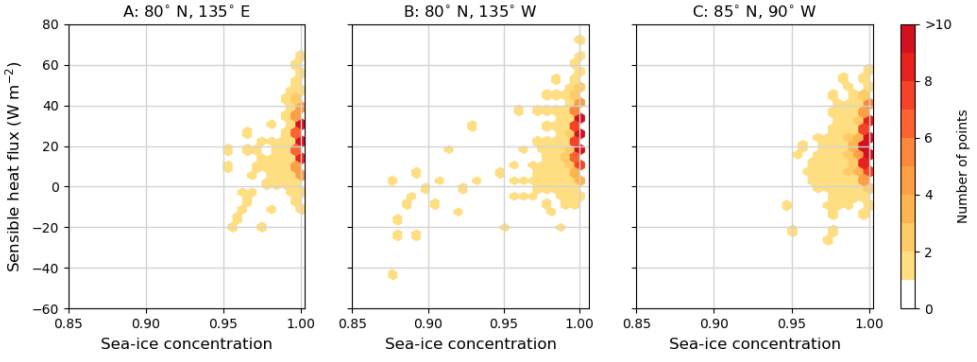

Figure 7. Daily sea-ice concentration and sensible heat flux in three selected grid cells from dark-grey areas indicated in Figure 6, NCEP/CFSR data, days in NDJ months in 1980–2000 (1932 days). **A**: Grid cell nearest to 80° N, 135° E; **B**: Grid cell nearest to 80° N, 135° W; **C**: Grid cell nearest to 85° N, 90° W.

study period, leading to a stronger statistical relationship between SIC and LHF.

Also for SHF, the change in the flux per unit of SIC (slope of the regression line) depended on the season, region, and decadal period (Figures 6, S6–S8). As in the case of SIC/LHF relationship, SIC and SHF were positively correlated in the

https://doi.org/10.5194/egusphere-2023-1131
Preprint. Discussion started: 6 July 2023

Arctic in NDJ (shades of red in Figure 6: i–iv), meaning less sea ice – more upward (negative) SHF. These results are also consistent with the theoretical expectations, as mentioned above: the sea is considerably warmer than the near-surface air in the cold seasons (NDJ, FMA) and, when the insulating sea-ice layer retreats, a large amount of upward SHF is released. The strength of the SIC/SHF correlation ranged from around 300 W m^{-2} SHF per unit of SIC in JRA-55 data (keeping in mind the limited area where it was possible to analyse the relationship) to around 800 W m^{-2} SHF per unit of SIC in ERA5, NCEP/CFSR, and MERRA-2. Similarly to SIC/LHF, there were dark grey areas (grid cells) in our results of SIC/SHF regression analysis, where the linear bilateral ODR model did not converge. As we mentioned above, in the case of JRA-55 (Figures 4 and 6: ii and vi), the failure of the model was caused by the binary representation of SIC in this reanalysis which makes it impossible for the model to explain the variations in LHF or SHF by variations in SIC. In Figure 7, using grid cells from dark grey areas from NCEP/CFSR data (as indicated in Figure 6), we show that in cold seasons, the reason for the model failure is similar also in reanalyses with fractional representation of SIC – very low SIC variability and high SHF variability. In these selected grid cells the SIC mostly varied only between 0.95 and 1, while SHF showed variability between -20–60 W m^{-2}. On most days (highest density of points, darkest orange/red), the SIC was 1 and SHF 0–30 W m^{-2}, resulting in no clear bilateral relationship.

Comparably with the SIC/LHF relationship, we also found positive correlation for SIC/SHF in FMA and partly ASO (shades of red in Figures S6 and S8: i–iv). The areas where the linear ODR model did not converge expanded considerably in FMA compared to NDJ, probably due to less variation in SIC during FMA (before the melting starts) compared to NDJ (with the sea typically just starting to freeze in November). The fact that there are more dark-grey areas in Figures 6 and S6 (SIC/SHF relationship, NDJ, FMA) than Figures 4 and S3 a (SIC/LHF relationship, NDJ, FMA) can be attributed to greater variability in SHF than LHF in the Arctic during these seasons, making it harder for the model to fit a regression line when SIC is very high. In MJJ, the SIC/SHF relationship also turned into a negative correlation (shades of blue in Figure S7), meaning less SIC – more downward (positive) SHF. We observed similar spatial distribution of the correlation strength as in SIC/LHF results for MJJ, with the maximum slope of the regression line in the Central Arctic (around 400 W m^{-2} per unit of SIC in ERA5 and MERRA-2, and up to 800 W m^{-2} per unit of SIC in NCEP/CFSR). The summer change of the slope sign can be explained analogically to the SIC/LHF relationship: the open water at the sea-water freezing point (-1.8 °C) is colder than the summer ice surface temperature at about the snow/ice melting point (0 °C). Therefore opening leads (less sea ice) induces more downward (positive) SHF in reanalyses.

The SIC effect on SHF weakened between 1980–2000 and 2001–2021 in most of the Arctic and strengthened in some parts of the Central Arctic and Beaufort Sea across all the seasons (shades of blue in Figures 6, S6, S8: v–viii; shades of red in Figure S7: v-viii), very similarly to the SIC/LHF relationship. The same explanation of this trend is valid for the change in SIC/SHF relationship: Increasing surface temperature of the sea ice reduces the surface temperature difference between ice and water, directly contributing to lower sensitivity of SHF to SIC. The (statistically) stronger relationship between SIC and SHF in Central Arctic and Beaufort Sea in 2001–2021 compared to 1980–2000 (shades of red in Figures 6, S6, S8: v–viii; shades of blue in Figure S7: v-viii) can again be assigned to the greater variability of SIC in these regions in the latter study period.

https://doi.org/10.5194/egusphere-2023-1131
Preprint. Discussion started: 6 July 2023

3.3 Multiple drivers of surface turbulent fluxes

To assess more drivers of the surface turbulent fluxes in reanalyses (as shown in the fluxes' bulk parameterisation in Eqs. (1) and (2)), we further performed linear multilateral ordinary-least-square regression (OLSR) analyses utilizing SIC, specific-humidity difference (Q_{diff}, Q_s minus Q_{2m}), and wind speed in 10m (WS_{10m}) as explanatory variables for variance in LHF; and SIC, temperature difference (T_{diff}, T_s minus T_{2m}), and wind speed in 10m (WS_{10m}) as explanatory variables for SHF variance. As an outcome of these analyses, we studied the variance in LHF or SHF (vLHF, vSHF) explained by the model (coefficient of determination, R^2) overall, and the proportion of the overall R^2 explained by each of the three drivers mentioned above.

Besides the decline in the sea-ice extent, we found both the overall and partial values of R^2 in 1980–2000 quantitatively very similar to those in 2001–2021 within all reanalyses, seasons and both LHF and SHF (Figures 8, S9–S23).
During the cold seasons (NDJ, FMA), the model explained around 80 % of vSHF, with similar spatial distribution in ERA5, JRA-55, and MERRA-2 (Figures 8, S9-S11). The partial R^2 also had similar values within these three reanalyses – around 20 % vSHF explained by SIC, around 50 % explained by T_{diff}, and around 10 % by WS_{10m}. In NCEP/CFSR in NDJ and FMA, however, nearly everywhere outside of the marginal-ice zone (MIZ), the model explained only around 40–50 % vSHF overall. While in these regions, the partial R^2 explained by SIC and WS_{10m} had about the same values as in the remaining three reanalyses, the partial R^2 for T_{diff} only reached values around 20–30 %. During the warm seasons (MJJ, ASO; Figures S12–S15), however, both overall and partial R^2 in NCEP/CFSR were about the same as in other reanalyses (about 70–80 % overall, around 10 % for SIC, 60 % for T_{diff}, and mostly $<$10 % for WS_{10m}). Hence, the cold-seasons difference in NCEP/CFSR results are likely due to the role of snow on the sea ice (which is existing and modelled in this reanalysis unlike in the other ones). Insulation by snow causes lower T_s because it reduces upward conductive heat flux from the ocean under the sea ice to the snow surface. Lower T_s reduces T_{diff} in very cold NDJ and FMA conditions in the Arctic. At the same time, when a lead opens, the difference between T_s of the snow and T_s of the water is much larger than the difference between the T_s of bare sea ice and water, resulting in larger magnitude of upward SHF than in the case of bare sea-ice surface compared to open water. In NDJ and FMA, this should make variance in SIC more important in explaining vSHF to account for the lower importance of T_{diff} in NCEP/CFSR than the remaining reanalyses. However, according to our results in Figures 8, S9–S11, this was mostly not the case. As we presented for bilateral relationships between SIC and SHF in Figures 6 and S6, the linear ODR model using NCEP/CFSR data did not converge in large areas of the marine Arctic in NDJ and even larger areas in FMA presumably due to very low variability in the SIC and large variability in SHF, which points to the difficulty faced by this kind of model in reproducing cold-seasons surface and near-surface-air conditions using NCEP/CFSR data.

The vLHF explained by the linear multilateral OLSR in warm seasons (MJJ, ASO; Figures S20–S23) was very similar to that for vSHF for both study periods and all reanalyses – around 80 % overall, around 10–20 % for SIC, 50–60 % for Q_{diff}, and around 10 % for WS_{10m}. In NDJ and FMA (Figures S16–S19), we also came across lower overall (and Q_{diff}) R^2 – around 40 % (and $<$10 %) in NCEP/CFSR results in the areas of SIC/LHF linear model failure. In other reanalyses for these cold seasons, the overall vLHF explained by the model had about the same values as in the case of vSHF, although, the partial R^2

https://doi.org/10.5194/egusphere-2023-1131
Preprint. Discussion started: 6 July 2023

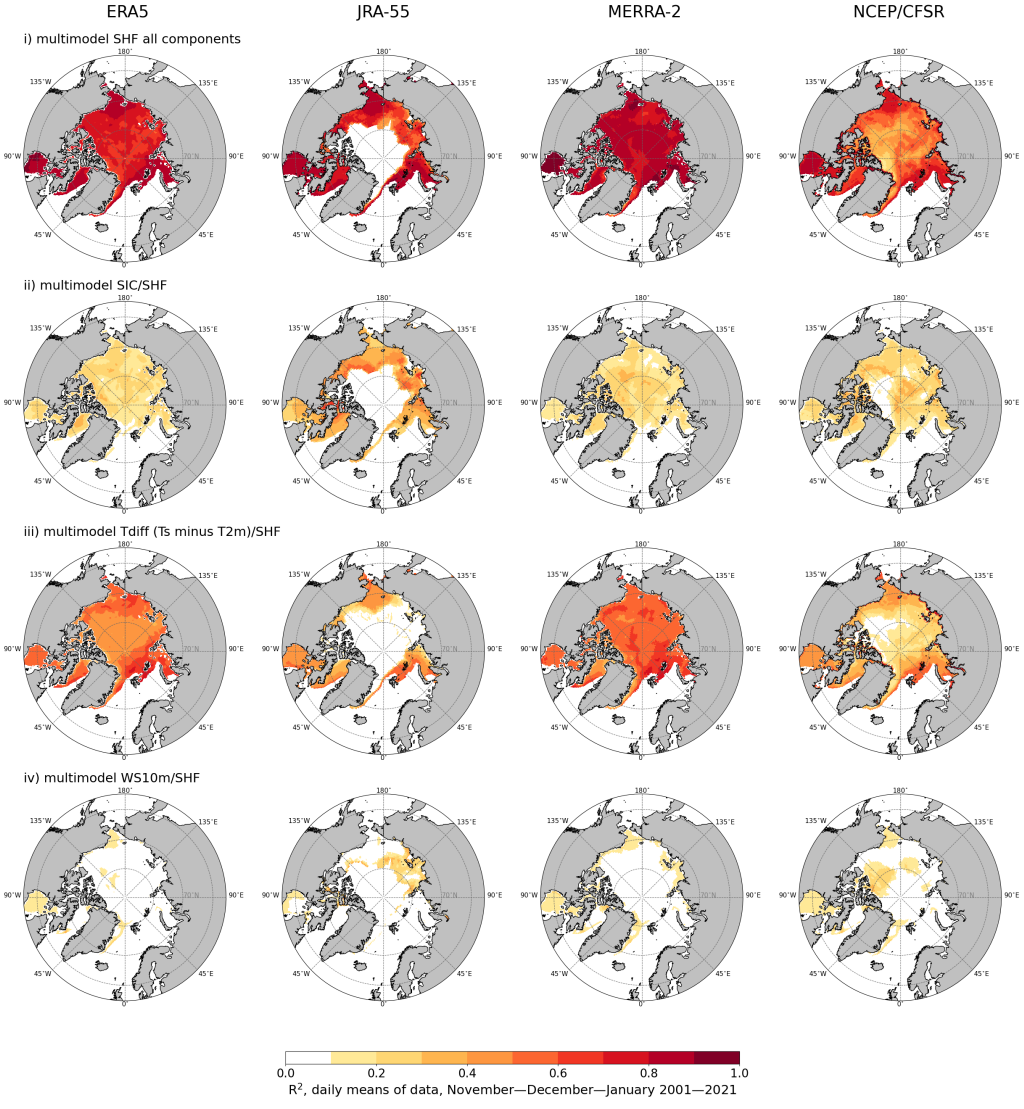

Figure 8. Proportion of variance in the sensible heat flux (vSHF) explained by the linear ordinary-least-square regression model (coefficient of determination, R^2); daily means of data, NDJ, 2001–2021. Row **i** - vSHF explained by all components: SIC/temperature difference (T_s minus T_{2m}, T_{diff})/wind speed (10 m, WS_{10m}); row **ii** - vSHF explained by the SIC/SHF component of the model; row **iii** - vSHF explained by the T_{diff}/SHF component of the model; row **iv** - vSHF explained by the WS_{10m}/SHF component of the model. Only grid cells with a mean of SIC > 0.5 were considered.

https://doi.org/10.5194/egusphere-2023-1131
Preprint. Discussion started: 6 July 2023

for SIC were higher (around 40 % in NDJ and around 30 % in FMA) and the partial R^2 for Q_{diff} accordingly lower. Variations in WS_{10m} explained on average more vLHF than vSHF – around 10–20 %.

4 Discussion and Conclusions

In most Arctic basins, we found the highest SIC in NCEP/CFSR and JRA-55 data, whereas the values in ERA5 and MERRA-2 were lower and close to each other. The magnitude of the differences was up to 0.15, but typically around 0.05 (Figure 2), similar to the average differences between reanalyses in the Arctic Ocean shown in Collow et al. (2020). Differences in SIC of the order of 0.05 to 0.15 may generate large differences in turbulent surface fluxes, and the magnitude of these differences depends on the sensitivity of the fluxes to SIC. Our results indicated the highest sensitivity in NDJ and FMA: approximately 400 W m^{-2} in LHF and over 800 W m^{-2} SHF per unit of SIC (change of SIC from 0 to 1). These values varied between the reanalyses – e.g. for LHF in NDJ, in ERA5, JRA-55, and MERRA-2, they were approximately 200–300 W m^{-2} per unit of SIC, whereas it was as large as up to 600 W m^{-2} LHF per unit of SIC in NCEP/CFSR data. In warmer seasons, the sensitivity of turbulent surface fluxes to SIC was generally lower.

Large differences between reanalyses in their SIC values and in the sensitivity of turbulent surface fluxes to SIC (a) indicate challenges in representing atmosphere-sea ice interactions in NWP models, and (b) generate inaccuracies in diagnostic studies based on reanalyses products. Accurate modelling of atmosphere–sea ice interactions requires the most accurate information on SIC possible; however, even with perfect information on SIC, the different sensitivity of turbulent surface fluxes to SIC in reanalyses generates further uncertainties. These are related to the application of Eqs. (1) and (2) shown in Section 2. The NWP models used in the production of reanalyses have mutual differences in the height of their lowest atmospheric level, where the data on air potential temperature, specific humidity, and wind speed are taken. The height of the level affects the differences between the atmospheric and surface values, and the turbulent transfer coefficients for heat and moisture should be correctly adjusted to the height. The lowest level should be located within the lowest 10 % of the atmospheric boundary layer (ABL), where the turbulent fluxes can be assumed to be constant in height. As the ABL height varies in space and time, the lowest model level is often located higher. In such cases, the Monin-Obukhov similarity theory (the basis for Eqs. (1) and (2)) is not valid. This is a particularly serious problem over thick sea ice in cold seasons, when stable stratification prevails and the ABL is very shallow. In such conditions, there is a lot of uncertainty in the dependence of the turbulent mixing on the stratification (Andreas et al. (2010); Grachev et al. (2012)). In particular, the transition from weakly stable to very stable stratification leads to a decrease in the magnitude of SHF even if the temperature difference between the air and the surface increases (Malhi, 1995), which may result in uncertainties of 10–20 K in T_{2m} (Uppala et al., 2005). Further, the flux parameterisation includes challenges related to the vertical distribution of heat originating from narrow open leads (Lüpkes et al., 2012), and to the limited representativeness of the grid-averaged values of air potential temperature, specific humidity and wind speed over the open and ice-covered parts of the grid cell (Vihma et al., 1998). As the NWP models applied in the production of the ERA5, JRA-55, MERRA-2, and NCEP/CFSR reanalyses have different vertical resolutions and different stability dependence of turbulent exchanges coefficients, it is understandable that the reanalyses differ in sensitivity to SIC.

https://doi.org/10.5194/egusphere-2023-1131
Preprint. Discussion started: 6 July 2023

The differences in LHF and SHF, generated by differences in SIC and flux parameterisations, have strong impacts on the atmosphere, above all in cold-seasons conditions (NDJ, FMA) when the SIC is close to one. According to modelling experiments by (Lüpkes et al., 2008), in winter under clear skies, a SIC decrease of 1 % caused a T_{10m} increase of 3.5 K when the air mass flew long enough (48 h) over the zone of a high SIC. During cold-air outbreaks from the Antarctic sea ice zone, modelled T_{2m} may vary by more than 10 K depending on the SIC algorithm applied (Valkonen et al., 2008). Warming and reduction of stratification in the Arctic ABL also makes the atmosphere more prone to cyclogenesis (Jaiser et al., 2012). Such local and regional impacts in the sea ice zone may have far-reaching effects beyond the polar regions. Sea-ice decline in the Arctic contributes to the Arctic amplification of climate warming, reducing the meridional temperature gradient between the Arctic and mid-latitudes. This impacts mid-latitude weather and climate, although the magnitude of the impacts and their distinction from natural variability is still under debate (Cohen et al., 2020).

The SIC in reanalyses does not include information on the spatial distribution of sea ice and open water within a grid cell. For example, if SIC is 0.5 we do not know whether there is a distinct ice margin dividing the grid cell in equal portions of sea ice and open sea or if there are numerous small leads whose total area sums up to half of the grid cell. The impacts of the ice-water distribution on turbulent surface fluxes may depend on the season, region, and weather conditions via complex interaction of processes. In the case of cold-air outbreaks in cold seasons, when the sensitivity of SHF and LHF to SIC is largest, a distinct ice margin (with only sea ice on one side and only open water on the other side) typically results in a situation when SHF and LHF are largest right downwind of the ice margin, and then decrease with fetch over the open sea, as the near-surface air becomes warmer and more humid (e.g. Lüpkes and Schlünzen (1996)). In a similar weather situation but with the SIC associated with a series of narrow leads, the near-surface air is not expected to get as warm and moist, because part of the heat and moisture is returned to ice via downward turbulent fluxes over the patches of ice in between the leads, which allows larger SHF and LHF over the leads. However, comparing the turbulent surface fluxes averaged over the grid cell between these two exemplary cases would require sophisticated large-eddy simulation experiments. A theoretical argument favouring larger grid-averaged fluxes in the latter case is that the alternations between the leads and sea ice increase the surface roughness due to the form drag generated by floe edges (Lüpkes and Gryanik, 2015). This enhances the turbulent transfer not only for momentum but also for sensible and latent heat (Elvidge et al., 2023). In any case, even if the reanalysis products would include information on the spatial distributions of sea ice and open water within a grid cell, the SIC itself is an a oversimplification of the true situation, where the sea ice in a grid cell typically has a range of thicknesses, each with different surface temperature and, hence, SHF and LHF.

Comparing the effects of SIC and other factors on LHF and SHF, it is evident that air-surface differences in temperature and specific humidity explain the flux variations better than SIC does. This is natural, as the air-surface differences are the basis for flux parameterisations in models. However, SIC plays a key role in controlling the surface temperature and the surface (saturation) specific humidity, which have constant (freezing-point related) values over areas of open water in the sea-ice zone (farther south, the sea surface temperature may strongly exceed the freezing point). Accordingly, the air-surface differences in temperature and specific humidity are strongly affected by SIC. Wind speed explained only 10 to 20 % of the turbulent surface

https://doi.org/10.5194/egusphere-2023-1131
Preprint. Discussion started: 6 July 2023

fluxes variances, which we interpret as follows. Under constant air-surface differences in temperature and specific humidity, the magnitude of turbulent fluxes increases with increasing wind speed, as seen from Eqs. (1) and (2). However, in events of upward fluxes, the wind effect results in decrease of the fluxes, whereas in events of downward fluxes, the fluxes increase. The cancelling effects keep the degree of explanation small. It does not vanish because events with a high air temperature and specific humidity over the Arctic Ocean typically occur under strong winds (Walsh and Chapman (1998); Vihma and Pirazzini (2005)), favouring increase of the downward turbulent fluxes.

As expected, all four reanalyses agreed on the general decrease of SIC over the 42-year study period. However, anomalies occurred in the Central Arctic in NDJ, FMA, and MJJ, and in the Beaufort Sea in NDJ and FMA, where SIC remained the same or became higher in the second half of the study period, by up to 0.01 (around 1 % of the value in 1980–2000). These results are likely connected to the thinning of the Arctic sea ice in recent decades, which makes it more prone to ridging, rafting, and fast drift (Rampal et al., 2009). The exact mechanisms for the SIC increase remain unclear, but possibilities include regionally increased convergence of ice drift, associated with the closing of leads. Over the Barents and Kara Seas in ASO, we detected only a minor decadal increase in LHF and SHF (Tables 4 and S1), although the sea-ice decline has been very large. We interpret this as a consequence of increased transport of moist, warm air masses to the Arctic (Woods and Caballero, 2016) also associated with increasingly meridional cyclone tracks (Wickström et al., 2020).

We found that the effect of SIC on both LHF and SHF weakened between the study periods and present the following explanations for this finding. Considering leads in environment of high SIC, the surface temperature of ice has increased whereas the underlying sea temperature has remained the same (at the sea-water freezing temperature of approximately -1.8 °C). As leads open and close frequently, the lead surface temperature remains close to -1.8 °C. Hence, the difference in the surface saturation specific humidities between the sea ice and open water has decreased, directly contributing to a decreased sensitivity of LHF to SIC, and analogously for SHF due to decrease in the surface temperatures of sea ice and leads. Considering areas where the sea ice has declined considerably or completely disappeared, in the latter study period, there is very small or no effect of SIC on LHF and SHF. Mostly in the Central Arctic, however, we found areas of increased effect of SIC on LHF and SHF between 1980–2000 and 2001–2021. We interpret this as a result of an increased variability of SIC in these areas during the latter study period, leading to a stronger statistical relationship between SIC and the turbulent surface fluxes

The results generally indicated signs of decadal-scale improvement in the mutual agreement between reanalyses. The magnitudes of the mean biases in LHF and SHF between ERA5 and the other reanalyses have decreased in nearly all basins and seasons. As the model and data assimilation system is the same over the entire reanalysis period, the better agreement may result from more data available for assimilation. This must be mostly due to more available satellite data, as increases in the amount of in-situ observations from the Arctic have been restricted to short periods, such as The Year of Polar Prediction (YOPP) Special Observation Periods in February–March and July–September in 2018 and The Multidisciplinary drifting Observatory for the Study of Arctic Climate (MOSAiC) field campaign in 2019–2020.

Our study expanded the knowledge on the effects of Arctic sea-ice concentration on the turbulent surface fluxes of sensible and latent heat, as represented in four atmospheric reanalyses. We quantified the uncertainties in these effects arising from

https://doi.org/10.5194/egusphere-2023-1131
Preprint. Discussion started: 6 July 2023

differences in SIC and in the sensitivity of the turbulent surface fluxes to SIC. A logical next step is to study the effects of Arctic SIC on radiative surface fluxes in atmospheric reanalyses.

Code and data availability. https://doi.org/10.5281/zenodo.7978071, https://doi.org/10.5281/zenodo.7965919, https://a3s.fi/uhlitere-2000789-pub/* (To download a desired file, the name of it must be entered after the last forward slash, instead of *. Names of files can be found in codes or in the list of files at https://a3s.fi/swift/v1/AUTH_ea49151ae29449449d8e7cde1367e03a/uhlitere-2000789-pub/. Data description can be found at https://a3s.fi/uhlitere-2000789-pub/README_data.odt)

Author contributions. TU prepared the manuscript with contributions of TV, PU, and AK. TV designed the concept of the study with contributions of PU, AK, and TU. PU developed the code with the contribution of TU. TU collected and processed data and performed analyses.

Competing interests. The authors declare that they have no conflict of interest.

Acknowledgements. TU is a University-funded Doctoral Researcher at the University of Helsinki. The work of AK, PU, and TV was supported by the European Commission, Horizon 2020 Framework Programme (PolarRES; grant no. 101003590).

Hersbach et al. (2023) was downloaded from the Copernicus Climate Change Service (C3S) Climate Data Store (2023). The results contain modified Copernicus Climate Change Service information 2022. Neither the European Commission nor ECMWF is responsible for any use that may be made of the Copernicus information or data it contains. Furthermore, we acknowledge the providers of the data of the other three reanalyses used in our study: Japan Meteorological Agency, the National Center for Atmospheric Research (JRA-55, NCEP/CFSR, CFSv2), and the Global Modeling and Assimilation Office (MERRA-2).

https://doi.org/10.5194/egusphere-2023-1131
Preprint. Discussion started: 6 July 2023

References

Andreas, E. L., Persson, P. O. G., Grachev, A. A., Jordan, R. E., Horst, T., Guest, P. S., and Fairall, C.: Parameterizing Turbulent Exchange over Sea Ice in Winter, J. Hydrometeorol, 11, 87–104, https://doi.org/10.1175/2009JHM1102.1, 2010.

Aue, L., Vihma, T., Uotila, P., and Rinke, A.: On the warm bias in atmospheric reanalyses induced by the missing snow over Arctic sea-ice, Geophysical Research Letters, 49, https://doi.org/10.1029/2022GL100051, 2022.

Boggs, P. T., Donaldson, J. T., Schnabel, R. B., and Spiegelman, C. H.: A Computational Examination of Orthogonal Distance Regression, Journal of Econometrics, 38, 169–201, https://www.sciencedirect.com/science/article/pii/0304407688900322, 1988.

Bosilovich, M. G., Akella, S., and Coy, L. e. a.: MERRA-2: Initial evaluation of the climate, https://gmao.gsfc.nasa.gov/pubs/docs/Bosilovich803.pdf, 2015.

Bretherton, C. S., Widmann, M., Dymnikov, V. P., Wallace, J. M., and Bladé, I.: The Effective Number of Spatial Degrees of Freedom of a Time-Varying Field, Journal of Climate, 12, 1990–2009, https://journals.ametsoc.org/view/journals/clim/12/7/1520-0442_1999_012_1990_tenosd_2.0.co_2.xml, 1999.

Chung, E.-S., Ha, K.-J.and Timmermann, A., Stuecker, M. F., Bodai, T., and Lee, S.-K.: Cold-season Arctic amplification driven by Arctic ocean-mediated seasonal energy transfer., Earth's Future, 9, https://doi.org/10.1029/2020EF001898, 2021.

Claussen, M.: Local advection processes in the surface layer of the marginal ice zone, Boundary-Layer Meteorol, 54, 1–27, https://doi.org/10.1007/BF00119409, 1991.

Cohen, J., Zhang, X., Francis, J., Jung, T., Kwok, R., Overland, J., Ballinger, T. J., Bhatt, U. S., Chen, H. W., Coumou, D., Feldstein, S., Gu, H., Handorf, D., Henderson, G., Ionita, M., Kretschmer, M., Laliberte, F., Lee, S., Linderholm, H. W., Maslowski, W., Peings, Y., Pfeiffer, K., Rigor, I., Semmler, T., Stroeve, J., Taylor, P. C., Vavrus, S., Vihma, T., Wang, S., Wendisch, M., Wu, Y., and Yoon, J.: Divergent consensuses on Arctic amplification influence on midlatitude severe winter weather., Nature climate change, pp. 20–29, https://doi.org/10.1038/s41558-019-0662-y, 2020.

Collow, A. B. M., Cullather, R. I., and Bosilovich, M. G.: Recent Arctic Ocean Surface Air Temperatures in Atmospheric Reanalyses and Numerical Simulations, Journal of Climate, 33, 4347–4367, https://journals.ametsoc.org/view/journals/clim/33/10/jcli-d-19-0703.1.xml, 2020.

Dai, A., Luo, D., Song, M., and Liu, J.: Arctic amplification caused by sea-ice loss under increasing CO2., Nature communications, 10, https://doi.org/10.1038/s41467-018-07954-9, 2002.

ECMWF: IFS Documentation CY41R2 - Part IV: Physical Processes, 4, ECMWF, https://doi.org/10.21957/tr5rv27xu, 2016.

Elvidge, A. D., Renfrew, I. A., Edwards, J. M., Brooks, I. M., Srivastava, P., and Weiss, A. I.: Improved simulation of the polar atmospheric boundary layer by accounting for aerodynamic roughness in the parameterization of surface scalar exchange over sea ice., Journal of Advances in Modeling Earth Systems, 15, https://doi.org/10.1029/2022MS003305, 2023.

Gelaro, R., McCarthy, W., and Suárez, M. J. e. a.: The Modern-Era Retrospective Analysis for Research and Applications, Version 2 (MERRA-2), Journal of Climate, 30, 5419–5454, 2017.

GMAO, Global Modeling, A. O.: Tavg1_2d_flx_Nx: MERRA-2 2D, 1-Hourly, Time-Averaged, Single-Level Assimilation, Single-Level Diagnostics., https://doi.org/10.5067/7MCPBJ41Y0K6, 2015a.

GMAO, Global Modeling, A. O.: Tavg1_2d_slv_Nx: MERRA-2 2D, 1-hourly, Time-Averaged, Single-Level Assimilation,Surface Flux Diagnostics V5.12.4, https://doi.org/10.5067/VJAFPLI1CSIV, 2015b.

https://doi.org/10.5194/egusphere-2023-1131
Preprint. Discussion started: 6 July 2023

Good, S., Fiedler, E., Mao, C., Martin, M. J., Maycock, A., Reid, R., Roberts-Jones, J., Searle, T., Waters, J., While, J., and Worsfold, M.: The Current Configuration of the OSTIA System for Operational Production of Foundation Sea Surface Temperature and Ice Concentration Analyses, Remote Sensing, 12, https://www.mdpi.com/2072-4292/12/4/720, 2020.

Grachev, A. A., Andreas, E. L., Fairall, C., Guest, P. S., and Persson, P. O. G.: Outlier problem in evaluating similarity functions in the stable atmospheric boundary layer, Bound.-Layer Meteorol., 144, 137–155, 2012.

Graham, R. M., Cohen, L., Ritzhaupt, N., Segger, B., Graversen, R. G., Rinke, A., Walden, V. P., Granskog, M. A., and Hudson, S. R.: Evaluation of Six Atmospheric Reanalyses over Arctic Sea Ice from Winter to Early Summer., Journal of Climate, 32, 4121–4143, https://doi.org/10.1175/JCLI-D-18-0643.1, 2019.

Gultepe, I., Isaac, G. A., Williams, A., Marcotte, D., and Strawbridge, K. B.: Turbulent heat fluxes over leads and polynyas, and their effects on arctic clouds during FIRE.ACE: Aircraft observations for April 1998, Atmosphere-Ocean, https://doi.org/10.3137/ao.410102, 2003.

Hersbach, H., Bell, B., Berrisford, P., Hirahara, S., Horányi, A., Muñoz Sabater, J., Nicolas, J., Peubey, C., Radu, R., Schepers, D., Simmons, A., Soci, C., Abdalla, S., Abellan, X., Balsamo, G., Bechtold, P., Biavati, G., Bidlot, J., Bonavita, M., and Thépaut, J.-N.: The ERA5 global reanalysis, Quarterly Journal of the Royal Meteorological Society, https://rmets.onlinelibrary.wiley.com/doi/10.1002/qj.3803, 2020.

Hersbach, H., Bell, B., Berrisford, P., Biavati, G., Horányi, A., J., M. S., Nicolas, J., Peubey, C., Radu, R., Rozum, I., Schepers, D., Simmons, A., Soci, C., Dee, D., and Thépaut, J.-N.: ERA5 hourly data on single levels from 1940 to present., https://doi.org/10.24381/cds.adbb2d47, 2023.

Iribarne, J. and Godson, W.: Atmospheric Thermodynamics, D. Reidel Publishing Company, 1973.

Ishii, M., Shouji, A., Sugimoto, S., and Matsumoto, T.: OBJECTIVE ANALYSES OF SEA-SURFACE TEMPERATURE AND MARINE METEOROLOGICAL VARIABLES FOR THE 20TH CENTURY USING ICOADS AND THE KOBE COLLECTION., International Journal of Climatology, 25, 865–879, https://rmets.onlinelibrary.wiley.com/doi/10.1002/joc.1169, 2005.

Jaiser, R., Dethloff, K., Handorf, D., and Cohen, J.: Impact of sea ice cover changes on the Northern Hemisphere atmospheric winter circulation, Tellus A: Dynamic Meteorology and Oceanography, 64, https://doi.org/10.3402/tellusa.v64i0.11595, 2012.

JMA, J. M. A.: JRA-55: Japanese 55-year Reanalysis, Daily 3-Hourly and 6-Hourly Data., https://doi.org/10.5065/D6HH6H41, 2013.

Kobayashi, S., Ota, Y., and Harada, Y. e. a.: The JRA-55 Reanalysis: General Specifications and Basic Characteristics, Journal of the Meteorological Society of Japan, 93, 5–48, https://doi.org/10.2151/JMSJ.2015-001, 2015.

Koster, R. D. and Suarez, M. J.: Modeling the land surface boundary in climate models as a composite of independent vegetation stands, J. Geophys. Res., 97, 2697—-2715, 1992.

Lim, W.-I., Park, H.-S., Stewart, A. L., and Seo, K.-H.: Suppression of Arctic sea ice growth in the Eurasian–Pacific seas by winter clouds and snowfall, Journal of Climate, 35, 669–686, https://doi.org/10.1175/JCLI-D-21-0282.1, 2022.

Lindsay, R., Wensnahan, M., Schweiger, A., and Zhang, J.: Evaluation of Seven Different Atmospheric Reanalysis Products in the Arctic., Journal of Climate, 27, 2588–2606, https://doi.org/10.1175/JCLI-D-13-00014.1, 2014.

Lüpkes, C. and Gryanik, V.: A stability-dependent parametrization of transfer coefficients for momentum and heat over polar sea ice to be used in climate models., Journal of Geophysical Research, 120, 2015.

Lüpkes, C. and Schlünzen, K. H.: Modelling the Arctic Convective Boundary-Layer with Different Turbulence Parameterizations., Boundary-Layer Meteorol., 79, 1996.

Lüpkes, C., Vihma, T., Birnbaum, G., and Wacker, U.: Influence of leads in sea ice on the temperature of the atmospheric boundary layer during polar night., Geophys. Res. Lett., 35, https://doi.org/10.1029/2007GL032461, 2008.

https://doi.org/10.5194/egusphere-2023-1131
Preprint. Discussion started: 6 July 2023

Lüpkes, C., Vihma, T., Birnbaum, G., Dierer, S., Garbrecht, T., Gryanik, V., Gryschka, M., Hartmann, J., Heinemann, G., Kaleschke, L., Raasch, S., Savijärvi, H., Schlünzen, K., and Wacker, U.: Mesoscale modelling of the Arctic atmospheric boundary layer and its interaction with sea ice, in: Arctic Climate Change - The ACSYS Decade and Beyond, edited by Lemke, P. and Jacobi, H.-W., vol. 43, Atmospheric and Oceanographic Sciences Library, 2012.

Maksimovich, E. and Vihma, T.: The effect of surface heat fluxes on interannual variability in the spring onset of snow melt in the central Arctic Ocean, Journal of Geophysical Research: Oceans, 117, https://doi.org/10.1029/2011JC007220, 2012.

Malhi, Y. S.: The significance of the dual solutions for heat fluxes measured by the temperature fluctuation method in stable conditions, Boundary-Layer Meteorol., 74, 389–396, 1995.

Matsumoto, T., Ishii, M., Fukuda, Y., and Hirahara, S.: Sea ice data derived from microwave radiometer for climate monitoring. Proceedings of the 14th Conference on Satellite Meteorology and Oceanography, Atlanta, USA., in: Presented at the 14th Conference on Satellite Meteorology and Oceanography, https://ams.confex.com/ams/Annual2006/techprogram/paper_101105.htm, 2006.

Michaelis, J., Lüpkes, C., Schmitt, A., and Hartmann, J.: Modelling and parametrization of the convective flow over leads in sea ice and comparison with airborne observations, Quarterly Journal of the Royal Meteorological Society, 147, https://doi.org/10.1002/qj.3953, 2021.

Morice, C. P., Kennedy, J. J., Rayner, N. A., W., P., J., Hogan, E., and Killick, R. E., e. a.: An updated assessment of near-surface temperature change from 1850: the HadCRUT5 data set., Journal of Geophysical Research: Atmospheres, 126, https://doi.org/10.1029/2019JD032361, 2021.

Overland, J. E., McNutt, S. L., Groves, J., Salo, S., Andreas, E. L., and Persson, P. O. G.: Regional sensible and radiative heat flux estimates for the winter arctic during the Surface Heat Budget of the Arctic Ocean (SHEBA) experiment, J. Geophys. Res., 105, 14 093—14 102, 2000.

Perovich, D. K., Light, B., Eicken, H., Jones, K. F., Runciman, K., and Nghiem, S. V.: Increasing solar heating of the Arctic Ocean and adjacent seas, 1979–2005: Attribution and role in the ice-albedo feedback, The Cryosphere, 34, https://doi.org/10.1029/2007GL031480, 2007.

Persson, P. O. G., W., F. C., L., A. E., Guest, P. G., and Perovich, D. K.: Measurements near the Atmospheric Surface Flux Group tower at SHEBA: Near-surface conditions and surface energy budget, J. Geophys. Res., 107, https://agupubs.onlinelibrary.wiley.com/doi/pdf/10.1029/2000JC000705, 2002.

Rampal, P., Weiss, J., and Marsan, D.: Positive trend in the mean speed and deformation rate of Arctic sea ice: 1979–2007, J. Geophys. Res., 114, 2009.

Saha, S., Moorthi, S., Pan, H.-L., Wu, X., Wang, J., Nadiga, S., Tripp, P., Kistler, R., Woollen, J., Behringer, D., Liu, H., Stokes, D., Grumbine, R., Gayno, G., Wang, J., Hou, Y.-T., Chuang, H.-Y., Juang, H.-M., Sela, J., and Goldberg, M.: The NCEP climate forecast system reanalysis, Bulletin of The American Meteorological Society, 91, https://doi.org/10.1175/2010BAMS3001.1, 2010.

Saha, S., Moorthi, S., Pan, H.-L., Wu, X., Wang, J., Nadiga, S., Tripp, P., Kistler, R., Woollen, J., Behringer, D., Liu, H., Stokes, D., Grumbine, R., Gayno, G., Wang, J., Hou, Y.-T., Chuang, H.-Y., Juang, H.-M. H., Sela, J., Iredell, M., Treadon, R., Kleist, D., Van Delst, P., Keyser, D., Derber, J., Ek, M., Meng, J., Wei, H., Yang, R., Lord, S., van den Dool, H., Kumar, A., Wang, W., Long, C., Chelliah, M., Xue, Y., Huang, B., Schemm, J.-K., Ebisuzaki, W., Lin, R., Xie, P., Chen, M., Zhou, S., Higgins, W., Zou, C.-Z., Liu, Q., Chen, Y., Han, Y., Cucurull, L., Reynolds, R. W., Rutledge, G., and Goldberg, M.: NCEP Climate Forecast System Reanalysis (CFSR) 6-hourly Products, January 1979 to December 2010., https://doi.org/10.5065/D69K487J, 2010.

https://doi.org/10.5194/egusphere-2023-1131
Preprint. Discussion started: 6 July 2023

Saha, S., Moorthi, S., Pan, H.-L., Wu, X., Wang, J., Nadiga, S., Tripp, P., Kistler, R., Woollen, J., Behringer, D., Liu, H., Stokes, D., Grumbine, R., Gayno, G., Wang, J., Hou, Y.-T., Chuang, H.-Y., Juang, H.-M. H., Sela, J., Iredell, M., Treadon, R., Kleist, D., Van Delst, P., Keyser, D., Derber, J., Ek, M., Meng, J., Wei, H., Yang, R., Lord, S., van den Dool, H., Kumar, A., Wang, W., Long, C., Chelliah, M., Xue, Y., Huang, B., Schemm, J.-K., Ebisuzaki, W., Lin, R., Xie, P., Chen, M., Zhou, S., Higgins, W., Zou, C.-Z., Liu, Q., Chen, Y., Han, Y., Cucurull, L., Reynolds, R. W., Rutledge, G., and Goldberg, M.: NCEP Climate Forecast System Version 2 (CFSv2) 6-hourly Products., https://doi.org/10.5065/D61C1TXF, 2011.

Saha, S., Moorthi, S., Wu, X., Wang, J., Nadiga, S., Tripp, P., Behringer, D., Hou, Y.-T., ya Chuang, H., Iredell, M., Ek, M., Meng, J., Yang, R., Mendez, M. P., van den Dool, H., Zhang, Q., Wang, W., Chen, M., and Becker, E.: The NCEP Climate Forecast System Version 2, Journal of Climate, 27, 2185 – 2208, https://journals.ametsoc.org/view/journals/clim/27/6/jcli-d-12-00823.1.xml, 2014.

Screen, J. A. and Simmonds, I.: The central role of diminishing sea ice in recent Arctic temperature amplification, Nature, 646, 1334–1337, https://doi.org/10.1038/nature09051, 2010.

Serreze, M. C., Barrett, A. P., Stroeve, J. C., Kindig, D. N., and Holland, M. M.: The emergence of surface-based Arctic amplification, The Cryosphere, 3, 11–19, https://tc.copernicus.org/articles/3/11/2009/tc-3-11-2009.pdf, 2009.

Taylor, K. E., Williamson, D., and Zwiers, F.: The sea surface temperature and sea-ice concentration boundary conditions for AMIP II simulations, in: PCMDI Report No. 60, https://pcmdi.llnl.gov/report/ab60.html, 2000.

Tsamados, M., Feltham, D., Petty, A., Schroeder, D., and Flocco, D.: Processes controlling surface, bottom and lateral melt of Arctic sea ice in a state of the art sea ice model, Phil. Trans. R. Soc. A, http://doi.org/10.1098/rsta.2014.0167, 2015.

Uppala, S. M., KÅllberg, P. W., Simmons, A. J., Andrae, U., Bechtold, V. D. C., Fiorino, M., Gibson, J. K., Haseler, J., Hernandez, A., Kelly, G. A., Li, X., Onogi, K., Saarinen, S., Sokka, N., Allan, R. P., Andersson, E., Arpe, K., Balmaseda, M. A., Beljaars, A. C. M., Berg, L. V. D., Bidlot, J., Bormann, N., Caires, S., Chevallier, F., Dethof, A., Dragosavac, M., Fisher, M., Fuentes, M., Hagemann, S., Hólm, E., Hoskins, B. J., Isaksen, L., Janssen, P. A. E. M., Jenne, R., Mcnally, A. P., Mahfouf, J.-F., Morcrette, J.-J., Rayner, N. A., Saunders, R. W., Simon, P., Sterl, A., Trenberth, K. E., Untch, A., Vasiljevic, D., Viterbo, P., and Woollen, J.: The ERA-40 reanalysis, Quarterly Journal of the Royal Meteorological Society, 131, https://doi.org/10.1256/qj.04.176, 2005.

Valkonen, T., Vihma, T., and Doble, M.: Mesoscale modelling of the atmospheric boundary layer over the Antarctic sea ice: a late autumn case study, Mon. Wea. Rev., 136, 1457–1474, 2008.

Vihma, T.: Subgrid parameterization of surface heat and momentum fluxes over polar oceans, J. Geophys. Res., 100, 1995.

Vihma, T. and Pirazzini, R.: On the factors controlling the snow surface and 2-m air temperatures over the Arctic sea ice in winter, Bound.-Layer Meteorol., 117, 73–90, 2005.

Vihma, T., Uotila, J., and Launiainen, J.: Air-sea interaction over a thermal marine front in the Denmark Strait, J. Geophys. Res., 103, 1998.

Vihma, T., Jaagus, J., Jakobson, E., and Palo, T.: Meteorological conditions in the Arctic Ocean in spring and summer 2007 as recorded on the drifting ice station Tara, Geophys. Res. Lett., 35, https://doi.org/10.1029/2008GL034681, 2008.

Walden, V. P., Hudson, S. R., Cohen, L., Murph, S. Y., and Granskog, M. A.: Atmospheric components of the surface energy budget over young sea ice : Results from the N-ICE2015 campaign., J. Geophys. Res. Atmos., 122, 8427—-8446, https://doi.org/10.1002/2016JD026091, 2017.

Walsh, J. E. and Chapman, W. L.: Arctic Cloud–Radiation–Temperature Associations in Observational Data and Atmospheric Re-analyses, J. Climate, 11, 3030–3045, 1998.

https://doi.org/10.5194/egusphere-2023-1131
Preprint. Discussion started: 6 July 2023

Wickström, S., Jonassen, M., Cassano, J. J., and Vihma, T.: Present temperature, precipitation and rain-on-snow climate in Svalbard, J. Geophys. Res. Atmospheres, 125, https://doi.org/10.1029/2019JD032155, 2020.

Woods, C. and Caballero, R.: The role of moist intrusions in winter Arctic warming and sea ice decline, J. Climate, 29, https://doi.org/10.1175/JCLI-D-15-0773.1, 2016.